Journal of Applied Fluid Mechanics, Vol. 5, No. 3, pp. 71-78, 2012.
Available online at www.jafmonline.net, ISSN 1735-3572, EISSN 1735-3645.
DOI: 10.36884/jafm.5.03.19447

Direct Two–Phase Numerical Simulation of Snowdrift Remediation using Three–Dimensional Deflection Fins

E. Maldonado[1] and M.W. Roth[1†]

[1]*Physics Department, University of Northern Iowa, Cedar Falls, IA, 50614, USA*

†*Corresponding Author Email:* rothm@uni.edu

(Received July 21, 2010; accepted November 4, 2010)

ABSTRACT

We present a versatile three – dimensional two – phase model for simulating snow drift relocation around buildings utilizing deflection fins of various shapes and sizes. The first phase involves numerically obtaining the air velocity profile around the building and fin using a velocity – pressure Navier – Stokes algorithm, while the second phase involves direct classical simulation of snowfall with particle – particle, particle – surface and one – way particle – gusting wind interactions introduced to control accumulation, erosion, clumping and drifting. Because the simulation technique is direct, it is potentially useful for storms and surfaces with widely varying conditions. We are also able to consider the effect of crosswinds.

Keywords: Deflection fin simulations, Direct snowfall simulations, Drifting simulations

NOMENCLATURE

A, B, C	computational cell dimensions
a	drag force coefficient
b	snowflake repulsion coefficient
c	snowflake sticking coefficient
g	acceleration of gravity
i,j,k	indices in x, y and z directions
m	mass of smowflake
n_x, n_y, n_z	number of x, y and z grid points
P	pressure
R	radius of snowflake
r_{ij}	separation between two snowflakes
u	x – component of velocity
v	y – component of velocity
v_{ij}	relative velocity of two snowflakes
$\vec{v}$	air velocity
W	z– component of velocity
x	horizontal coordinate
y	lateral coordinate
z	vertical coordinate
ρ	density of air
θ	Heaviside step function
Δt	time step
μ	kinematic viscosity of air

1. INTRODUCTION

Snow exhibits a wide range of characteristic dynamics, ranging from slow, almost vertical snowfall to the chaotic whirling and drifting seen in blizzards. Especially at extreme latitudes the drifting of snow can present significant challenges to people along many different fronts. Because computer simulations and mathematical modeling are very useful in understanding and even predicting the behavior of physical systems, especially ones that are associated with negative impact on people, researchers have mathematically investigated snowfall and its effects in one, two and three dimensions. The drifting and accumulation of snow in natural environments is directly related to avalanche danger; computer simulations have been used to estimate snow loading,(Lehning *et al.* 2000) transport (Doorschot *et al.* 2001) and drifting (Schneiderbauer *et al.* 2008; Lehning *et al.* 2002) in natural settings with the purpose of avalanche warning.(Lehning *et al.* 2000; Doorschot *et al.* 2001; Schneiderbauer *et al.* 2008; Lehning *et al.* 2002). In addition to snow behavior in natural settings, snow drifting in three dimensions around buildings of different shapes and aspect ratios (Akiyoshi *et al.* 1999; Kim *et al.* 1992; Beyers *et al.* 2008) and even cubes (Beyers *et al.* 2004) has been modeled.

Although it is very useful to understand the dynamics of snow drifting and transport, results of the processes themselves can present significant challenges to the activities of building occupants as well as to the structural integrity of buildings themselves. With such a purpose in mind, two recent studies (Sundsbø 1998; De Chant 2005) have been completed regarding two – dimensional numerical simulation of displacement of snowdrifts away from building walls using deflection

fins. The first involves a two – phase model which entails (i) numerical simulation of airflow due to the building and vertical deflection fin followed by (ii) a histogram cell model of snowfall accumulation and drifting. The geometry of the study (Sundsbø 1998) involves a 3m long deflection fin fixed 1.5m away from the top of a 3m high building and the results for deflecting the snow were very promising. The study also employed boundary conditions for turbulent flow (De Chant 2005) and an analytical solution for modeling snow accumulation involving various saltation, erosion and solidification processes.

The simulations and models for snow discussed above involve commercial codes (CFD; FLUENT; FLOW-3D, etc.) that calculate the air velocity profile coupled with analytical models that describe the snow profiles on relevant surfaces. Although the work discussed above is useful and well thought out, the very nature of snowfall suggests that direct numerical simulations incorporating snowflake-air, snowflake-snowflake and snowflake-surface interactions could reproduce essential elements of drifting and drift remediation. The second drift relocation study arose through concerns of drifting near two buildings on the University of Northern Iowa campus, and entails direct numerical simulation of the storm (Maldonado *et al.* 2012). It is also a two – phase model which incorporates (i) a pressure – velocity Navier – Stokes algorithm (Matyk *et al.* 2012) that solves for the air velocity field and (ii) direct numerical simulation of snow accumulation and erosion incorporating the interactions mentioned above using Newtonian dynamics and one – way coupling of the snowflakes to the air velocity field. We found that (i) the vertical placement of the fin affects the placement and dispersion of the snowdrift it creates, and the higher the fin is placed, the farther out from the building and more dispersed the drift is, (ii) The horizontal placement of the deflection fin affects how dispersed the snow drift will become, and (iii) the data suggests that a large fin (2 m – 3 m in length) placed within 1.6 m – 2 m from the building wall with half above the roof and half below could be very effective at preventing drifting near the building, which is consistent with results from previous work.(Sundsbø *et al.* 1998).

Many buildings present complexity in the boundary conditions they offer to the air as well as the snow particles; moreover the natural processes involved are inherently three – dimensional and so need for such drifting simulations in three dimensions is clear. Also it seems reasonable to believe that the simple direct numerical 2D simulation would also yield equally reasonable results in 3D because the natural processes and interactions are the same, and that the simulation could be easily adjusted for many different practical situations.

The purpose of the work reported here is (i) to extend our two – dimensional direct numerical snowfall simulations to three – dimensions, describing the model in detail and (ii) to report and discuss initial results of snowdrift relocation by deflection fins having novel shapes as well as the effects of crosswinds.

2. COMPUTATIONAL METHOD

2.1 Phase 1: Navier-Stokes Theory

The flow of air in this work is governed by the Navier Stokes equations for incompressible fluid flow:

$$\rho \frac{d\vec{v}}{dt} = -\vec{\nabla}P - \mu\nabla^2\vec{v} - \rho(\vec{v}\cdot\vec{\nabla})\vec{v} \tag{1}$$

Here, ρ is the fluid density (1.3 kg/m^3 for air), $\vec{v}$ is the velocity with Cartesian components $(v_x,v_y,v_z) = (u,v,w)$ at any point, P is the pressure at any point and μ is the fluid's dynamic viscosity ($1.983\text{x}10^{-5}$ kg/m s at temperature T = 300K for air). Eq. (1) deals with the momentum of the system and is a mathematical relationship stating that any acceleration in the fluid comes from three sources: pressure gradients, momentum diffusion through viscosity and momentum diffusion through convection.

Although required, Eq. (1) alone is not sufficient to model the system adequately. The equation of continuity

$$\frac{\partial\rho}{\partial t} + \rho\vec{\nabla}\cdot\vec{v} = 0 \tag{2}$$

is a statement of mass conservation which balances the change in density to the net fluid influx or outflux at any point in the system. Together, Eqs. (1) and (2) describe the physical behavior of the fluid phase of the system. A three – dimensional (3D) model is used because this work incorporates novel deflection fin shapes as well as side winds. Eqs. (1) and (2) then take the following explicit forms:

$$\rho\frac{du}{dt} = -\frac{dP}{dx} - \mu\left[\frac{d^2u}{dx^2}+\frac{d^2u}{dy^2}+\frac{d^2u}{dz^2}\right] - \rho u\frac{du}{dx} - \rho v\frac{du}{dy} - \rho w\frac{du}{dz} \tag{3a}$$

$$\rho\frac{dv}{dt} = -\frac{dP}{dy} - \mu\left[\frac{d^2v}{dx^2}+\frac{d^2v}{dy^2}+\frac{d^2v}{dz^2}\right] - \rho u\frac{dv}{dx} - \rho v\frac{dv}{dy} - \rho w\frac{dv}{dz} \tag{3b}$$

$$\rho\frac{dw}{dt} = -\frac{dP}{dz} - \mu\left[\frac{d^2w}{dx^2}+\frac{d^2w}{dy^2}+\frac{d^2w}{dz^2}\right] - \rho u\frac{dw}{dx} - \rho v\frac{dw}{dy} - \rho u\frac{dw}{dz} \tag{3c}$$

$$\frac{\partial\rho}{\partial t} + \rho\left[\frac{du}{dx}+\frac{dv}{dy}+\frac{dw}{dz}\right] = 0 \tag{4}$$

For a unique solution to Eqs. (3) and (4), boundary conditions are needed, which are shown in Table 1. The computational cell is chosen to be a rectangle of dimensions (A,B,C) = (40m, 20m, 12m) and the building has dimensions (10m, 13.3m, 3m); the deflection fin can be placed at any position within the computational cell and its lateral ends can be bent. Reasonable initial conditions $u(x,y,z,t=0) = u_0(x,y,z)$, $v(x,y,z,t=0) = v_0(x,y,z)$, $w(x,y,z,t=0) = w_0(x,y,z)$ and $P(x,y,z,t=0) = P_0(x,y,z)$ are specified which match the boundary conditions for the system being described.

In this work the high pressure is chosen such that the maximum gusting air speed above the building is about 15m/s, and is modulated by a sinusoidal function in time to represent gusting. The no – slip boundary condition implemented on the top of the simulation is of computational utility only and is far enough away from the building top that it does not significantly affect the action of the deflection fins.

Table 1 Phase 1 Boundary Conditions

	u	*V*	*w*	*P*
Ground	$u = 0$	$v = 0$	$w = 0$	$\frac{dP}{dz} = 0$
Ceiling	$u = 0$	$v = 0$	$w = 0$	$\frac{dP}{dz} = 0$
Inlet	$\frac{du}{dx} = 0$	$\frac{dv}{dx} = 0$	$\frac{dw}{dx} = 0$	$P = P_i(y,z)$
Outlet	$\frac{du}{dx} = 0$	$\frac{dv}{dx} = 0$	$\frac{dv}{dx} = 0$	$P = P_o(y,z)$
Front	$\frac{du}{dy} = 0$	$\frac{dv}{dy} = 0$	$\frac{dv}{dy} = 0$	$P = P_f(x,z)$
Back	$\frac{du}{dy} = 0$	$\frac{dv}{dy} = 0$	$\frac{dv}{dy} = 0$	$P = P_b(x,z)$
Interior barriers	$u = 0$	$v = 0$	$w = 0$	$\nabla_n P = 0$

2.2 Phase 2: Implementation

Figure 1 shows computational cell with relevant dimensions.

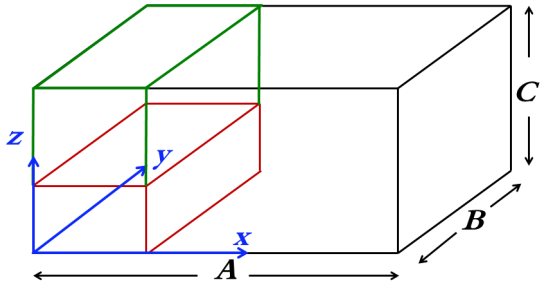

Fig. 1. The computational cell of dimensions (*A,B,C*) used in this work. The Cartesian coordinate system is in blue, the building outline is red and the region where snow is created is outlined in green. Not drawn to scale.

We follow a computational method for phase 1 similar to that shown in previous work (Maldonado *et al.* 2012) involving the SIMPLE algorithm (Matyk *et al.* 2012). The computational cell is divided into n_x spaces horizontally, n_y spaces laterally and n_z spaces vertically such that distance increments are $\Delta x = A/n_x - 1$, $\Delta y = B/n_y - 1$ and $\Delta z = C/n_z - 1$. The grid points are labeled as being either active or inactive, and the inactive cells are used to enforce any constant – value or free boundary conditions. The initial conditions are implemented for u_{ijk}, v_{ijk}, w_{ijk} and P_{ijk} for *i in* [0,n_x-1], *j in* [0,n_y-1] and *k* in [0,n_z-1]. Now the velocity field is updated using a discretized form of Eq. (3) over all active cells:

$$u_{i,j,k}^{n+1} = u_{i,j,k}^{n} - \left(\frac{\mu}{\rho}\left\{\frac{u_{i+1,j,k}^{n} - 2u_{i,j,k}^{n} + u_{i-1,j,k}^{n}}{(\Delta x)^2} + \frac{u_{i,j+1,k}^{n} - 2u_{i,j,k}^{n} + u_{i,j-1,k}^{n}}{(\Delta y)^2} + \frac{u_{i,j,k+1}^{n} - 2u_{i,j,k}^{n} + u_{i,j,k-1}^{n}}{(\Delta z)^2}\right\} + u_{i,j,k}^{n}\frac{u_{i+1,j,k}^{n} - u_{i-1,j,k}^{n}}{2\Delta x} + v_{i,j,k}^{n}\frac{u_{i,j+1.k}^{n} - u_{i,j-1,k}^{n}}{2\Delta y} + w_{i,j,k}^{n}\frac{u_{i,j.k+1}^{n} - u_{i,j,k-1}^{n}}{2\Delta z} + \frac{1}{\rho}\left\{\frac{P_{i+1,j,k}^{n} - P_{i-1,j,k}^{n}}{2\Delta x}\right\}\right)\Delta t \quad (5a)$$

$$v_{i,j,k}^{n+1} = v_{i,j,k}^{n} - \left(\frac{\mu}{\rho}\left\{\frac{v_{i+1,j,k}^{n} - 2v_{i,j,k}^{n} + v_{i-1,j,k}^{n}}{(\Delta x)^2} + \frac{v_{i,j+1,k}^{n} - 2v_{i,j,k}^{n} + v_{i,j-1,k}^{n}}{(\Delta y)^2} + \frac{v_{i,j,k+1}^{n} - 2v_{i,j,k}^{n} + v_{i,j,k-1}^{n}}{(\Delta z)^2}\right\} + u_{i,j,k}^{n}\frac{v_{i+1,j,k}^{n} - v_{i-1,j,k}^{n}}{2\Delta x} + v_{i,j,k}^{n}\frac{v_{i,j+1.k}^{n} - v_{i,j-1,k}^{n}}{2\Delta y} + w_{i,j,k}^{n}\frac{v_{i,j.k+1}^{n} - v_{i,j,k-1}^{n}}{2\Delta z} + \frac{1}{\rho}\left\{\frac{P_{i,j+1,k}^{n} - P_{i,j-1,k}^{n}}{2\Delta y}\right\}\right)\Delta t \quad (5b)$$

$$w_{i,j,k}^{n+1} = w_{i,j,k}^{n} - \left(\frac{\mu}{\rho}\left\{\frac{w_{i+1,j,k}^{n} - 2w_{i,j,k}^{n} + w_{i-1,j,k}^{n}}{(\Delta x)^2} + \frac{w_{i,j+1,k}^{n} - 2w_{i,j,k}^{n} + w_{i,j-1,k}^{n}}{(\Delta y)^2} + \frac{w_{i,j,k+1}^{n} - 2w_{i,j,k}^{n} + w_{i,j,k-1}^{n}}{(\Delta z)^2}\right\} + u_{i,j,k}^{n}\frac{w_{i+1,j,k}^{n} - w_{i-1,j,k}^{n}}{2\Delta x} + v_{i,j,k}^{n}\frac{w_{i,j+1.k}^{n} - w_{i,j-1,k}^{n}}{2\Delta y} + w_{i,j,k}^{n}\frac{w_{i,j.k+1}^{n} - w_{i,j,k-1}^{n}}{2\Delta z} + \frac{1}{\rho}\left\{\frac{P_{i,j,k+1}^{n} - P_{i,j,k-1}^{n}}{2\Delta z}\right\}\right)\Delta t \quad (5c)$$

The time step is chosen to be $\Delta t = 10^{-4}$ s, which is around the largest value that allows algorithm convergence and no significant change in results when doubled. Constant – value as well as constant derivative boundary conditions are implemented where required. The algorithm continuously repeats until results converge based upon the average fractional changes of the velocity components being less than a specified tolerance value. Since directly updating the velocity field does not ensure a divergence – free field as required but the continuity equation (Eq. 4) the pressure is corrected by adding P' to the pressure P_0 everywhere such that

$$\nabla^2 P' = -\vec{\nabla} \cdot \vec{v}.$$

In discretized form the pressure correction is calculated in an iterative loop as

$$P'^{n}_{i,j,k} = \frac{P'^{n}_{i,j-1,k}(\Delta y)^2 + P'^{n}_{i,j,k+1}(\Delta z)^2 + P'^{n}_{i,j,k-1}(\Delta z)^2}{2((\Delta x)^2 + (\Delta y)^2 + (\Delta z)^2)} + \frac{P'^{n}_{i+1,j,k}(\Delta x)^2 + P'^{n}_{i-1,j,k}(\Delta x)^2 + P'^{n}_{i,j+1,k}(\Delta y)^2}{2((\Delta x)^2 + (\Delta y)^2 + (\Delta z)^2)}$$

$$- \frac{u_{i+1,j}^{n} - u_{i-1,j}^{n}}{2\Delta x} - \frac{v_{i,j+1}^{n} - v_{i,j-1}^{n}}{2\Delta y} - \frac{w_{i,j+1}^{n} - w_{i,j-1}^{n}}{2\Delta z}.$$

The iterative loop also includes any constant value as well as constant derivative pressure conditions. When convergence is attained through similar criteria as

imposed on the velocity field, the correction is added to the pressure:

$$P^n_{i,j,k} = P^n_{0\,i,j,k} + P''^n_{i,j,k} \quad .$$

The velocity field is now updated so that it has zero divergence:

$$u^n_{i,j,k} = u^n_{i,j,k} - \frac{P^n_{i+1,j,k} - P^n_{i-1,j,k}}{2\Delta x}\Delta t$$

$$v^n_{i,j,k} = v^n_{i,j,k} - \frac{P^n_{i,j+1,k} - P^n_{i,j-1,k}}{2\Delta y}\Delta t.$$

$$w^n_{i,j,k} = w^n_{i,j,k} - \frac{P^n_{i,j,k+1} - P^n_{i,j,k-1}}{2\Delta z}\Delta t.$$

Then constant value as well as constant derivative velocity boundary conditions are again implemented.

2.3 Phase 2: Direct Simulation of Snow: Theory

All after the air velocity field $\vec{v}_{air}$ is calculated in phase 1, the points of drifting snow must be determined. We choose to model the classical trajectories using an initial boundary value problem involving a group of snowflakes modeled as spheres of radius *R*.

The differential equation governing the motion of each snowflake (*i*) is

$$m\frac{d\vec{v}_i}{dt} = -mg\hat{z} + a(\vec{v}_{air} - \vec{v}_i) + \sum_{j=1}^{n}\theta\left(1 - \frac{r_{ij}}{2R}\right)(b\hat{r}_{ji} + c\hat{v}_{ji}). \quad (6)$$

In the left hand side of Eq. (6) , $\vec{v}_i$ is the velocity vector of snowflake (i) in an orthogonal Cartesian coordinate system with the origin at the lower left corner of the building wall. The first term on the right hand side is a constant gravitational force in the vertical direction. The second term is a viscous drag term that takes into account the force that the air exerts on each snowflake which can be advancing, retarding or zero. The last term represents snowflake – snowflake interactions and is zero if the particles are not touching, as prescribed by the Heaviside step function θ. Within the sum, the $b\hat{r}_{ji}$ term expresses the normal force and is equal to a constant magnitude repulsive force directed along a line separating the flakes' centers if the snowflakes are touching. The $c\hat{v}_{ji}$ term is a friction term similar to that of previous work (De Chant *et al.* 2005) but is constant in magnitude and directed opposite the relative velocity of two touching snowflakes. Here $\hat{r}_{ji}$ is the unit vector pointing to snowflake (*i*) from snowflake (*j*), $\hat{v}_{ij}$ is the relative velocity vector pointing to snowflake (*j*) from snowflake (*i*). The values of important constants are shown in Table 2.

Table 2 Constants for Phase 2.

Constant	Value
m	$5\text{x}10^{-8}$ kg
g	9.8 m/s^2
a	9.8 N/kg
b	100N
c	20 N
R	1 cm

It should be noted that the size of the snowflakes are exaggerated so as to accelerate piling and accumulation but this difference from the size of real snowflakes do not alter the conclusions of the study. Such a result is attainable because, in this study the size explicitly affects the snowflake – snowflake interactions but not the snowflake – air interactions. Hence, the wind directs then to the same areas on the ground but they pile more readily.

The equation of motion (Eq. 5) is discretized and numerically integrated with respect to time utilizing Newton's method. As time advances, any snowflake may encounter a boundary, and so, in addition to the forces just discussed, there are three types of boundary conditions which must be implemented. First, the particle specularly reflects when it encounters a surface and its velocity component normal to the surface is reversed. Second, the surfaces perpendicular to gradient directions are free boundaries and so when a particle crosses through one it is returned to a random initial position. Finally, to account for friction with the ground, any snowflakes considered to be settled and moving slowly enough are stopped. The boundary conditions for phase 2 are summarized in Table 3.

Table 3 Phase 2 Boundary Conditions

Surface Type	Boundary Condition
Surfaces	
Walls and fin	Reversal of velocity component normal to the surface
Ground	sticking: $\vec{v}_i = 0$
Free boundaries	
Inlet, outlet, front, back	Return snowflake to random initial position
Drifting	
settled snowflakes	If $v_{xi} > 0.001$ m/s then $v_{xi} = 0$.

2.4 Phase 2: Implementation

Initially *n* spherical snowflakes are created in a rectangular region above the wall, placed at random positions within it and assigned initial velocities of zero. For the first quarter of the simulation, snow falls directly on the roof of the building because wind blowing snow off the loaded roof contributes to drifting in different way from saltation. When the remaining three quarters of the simulation begins, the air velocity (*u,v,w*) at the snowflake's position is determined using the Navier – Stokes algorithm of Phase I. Next the force on each snowflake is calculated using Eq. (5) and the acceleration is obtained by dividing the force by the snowflake's mass.

$$a_{ix} = \frac{a}{m}(u - v_{ix}) + \sum_{j=1}^{n}\theta\left(1 - \frac{r_{ij}}{2R}\right)\left(\frac{b}{m}\hat{r}_{ji}\cdot\hat{x} + \frac{c}{m}\hat{v}_{ji}\cdot\hat{x}\right) \quad (7a)$$

$$a_{iy} = \frac{a}{m}(v - v_{iy}) + \sum_{j=1}^{n}\theta\left(1 - \frac{r_{ij}}{2R}\right)\left(\frac{b}{m}\hat{r}_{ji}\cdot\hat{y} + \frac{c}{m}\hat{v}_{ji}\cdot\hat{y}\right) \quad (7b)$$

$$a_{iz} = -g + \frac{a}{m}(v - v_{iz}) + \sum_{j=1}^{n}\theta\left(1 - \frac{r_{ij}}{2R}\right)\left(\frac{b}{m}\hat{r}_{ji}\cdot\hat{z} + \frac{c}{m}\hat{v}_{ji}\cdot\hat{z}\right) \quad (7c)$$

Here θ is the Heaviside theta (step) function and appears to take into account that snowflake-snowflake interactions take place only for certain pair particle

separations. Then the trajectories of the flakes are obtained by numerically integrating the acceleration with respect to time using Newton's method:

$$v_{ix}^{n+1} = v_{ix}^{n} + a_{ix}\Delta t \quad (8a)$$

$$x_{i}^{n+1} = x_{i}^{n} + \left(\frac{v_{ix}^{n+1}+v_{ix}^{n}}{2}\right)\Delta t \quad (8b)$$

$$v_{iy}^{n+1} = v_{iy}^{n} + a_{iy}\Delta t \quad (8c)$$

$$y_{i}^{n+1} = y_{i}^{n} + \left(\frac{v_{iy}^{n+1}+v_{iy}^{n}}{2}\right)\Delta t \quad (8d)$$

$$v_{iz}^{n+1} = v_{iz}^{n} + a_{iz}\Delta t \quad (8e)$$

$$z_{i}^{n+1} = z_{i}^{n} + \left(\frac{v_{iz}^{n+1}+v_{iz}^{n}}{2}\right)\Delta t. \quad (8f)$$

A time step $\Delta t = 10^{-3}$ s is chosen so as to be large enough that the simulations complete in a reasonable time and yet small enough to give no significant change in results when doubled. After the system is advanced, any needed boundary conditions are implemented for a given snowflake and then the time integration loop continues. After a certain number of steps (in this case, one tenth of the total), another set of snowflakes are placed at initial random positions above the wall and the simulations continues until the total number of steps has been reached. Figure 2 illustrates the storm development, along with a typical ending configuration after 180,000 time steps and 200,000 particles have fallen. Since this work is not an intensive drifting study, the simulations were not run out so large drifts were obtained; rather statistically noticeable drifts were seen and then could be remediated. In addition, in cases of beginning drifting it is easier to see effects like shadowing and structure in the snow patterns.

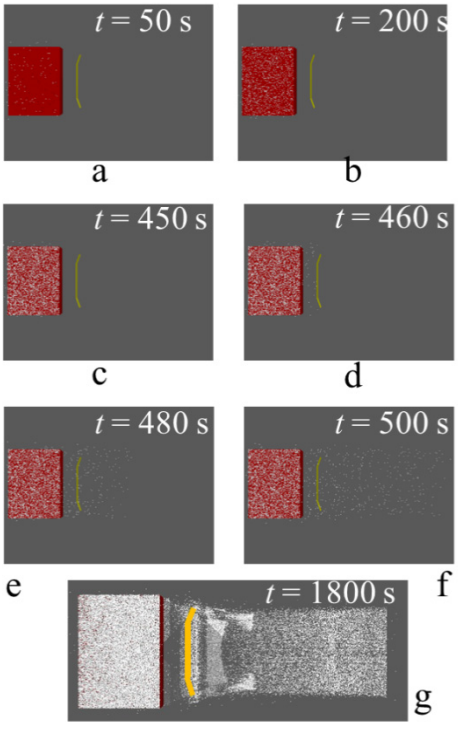

Fig. 2. Progression of the simulated snow storm, with snow falling vertically on the roof (a-c), the wind picking up and spreading the snow (d-f) and example final configuration with the deflection fin emphasized (g).

3. RESULTS AND DISCUSSION

Parameters in the simulation were adjusted so as to reproduce with reasonable accuracy the problematic drifting near the walls of the buildings on the UNI campus. Figure 3 shows the final snowfall profile on and around the building when a deflection fin is absent using visual rendering as well as height profile contours to emphasize subtle differences in the height field. Such results are utilized to not only validate the simulations but also to provide a reference for other systems with deflection fins in place. The results show problematic drifting close to the building as well as, surprisingly, high loading on the right edge of the roof. The depletion of accumulation on the ground a few meters downwind from the building has to do with the downdraft created by the building as the air rushes over it to the right.

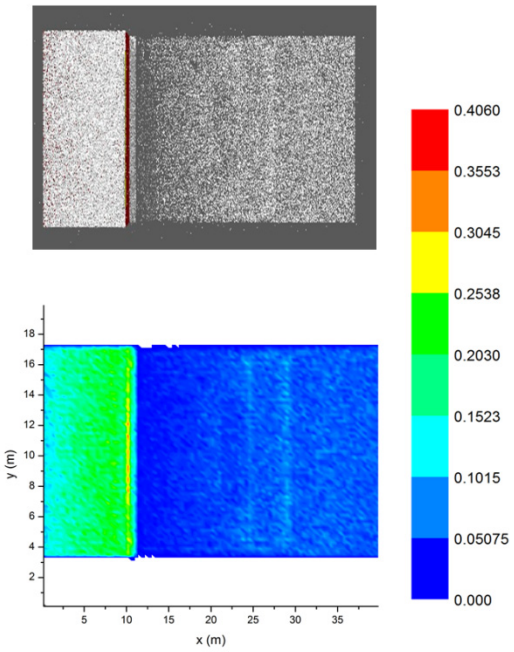

Fig. 3. Visual rendering (top) and contour map (bottom) of the snowfall depth pattern with no deflection fin present. In the contour map, red represents deepest snow and blue the shallowest relative to the horizontal surface below it. Values in the legend are calculated assuming realistic snowflake sizes and not exaggerated ones. Any regions of white indicate the absence of snow.

Figures 4, 5 and 6 show final snowfall profiles with straight fins placed at distances of 1.1m, 2.2 m and 3.3 m away from the building's edge, respectively. In each figure, the fin's center is coincident with the building's roof and the fin heights are varied (0.67 m – 5.36 m) with the fins centered vertically at the level of the building's roof.. Evidently, fins placed closest to the building have little positive effect on snow relocation, although the largest fins do result in slight relocation of the problematic drift nearest the building. Clearly, fins of medium height placed at intermediate distances (2.2 m) from the building do a better job of snow relocation, although placing them at 3.3 m from the building still has some positive effect. Such results are consistent

with previous work (Maldonado *et al.* 2012). The fins farthest from the building still deplete the problematic drift slightly but are too far past the downdraft created by the wall itself to have outstanding effects.

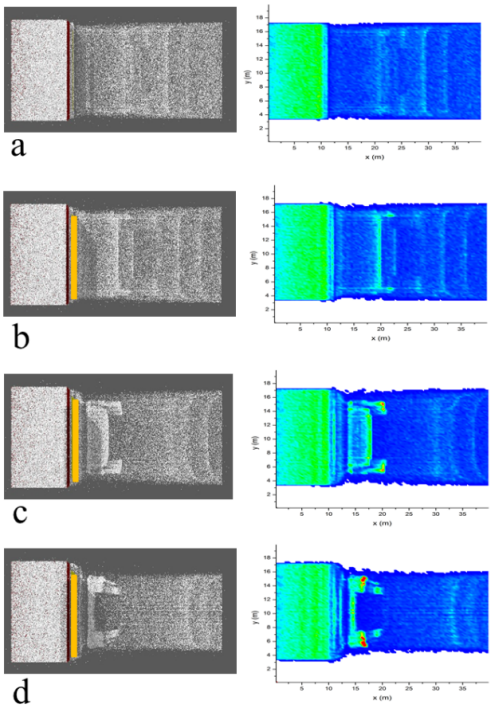

Fig. 4. Visual renderings (left column) and contour maps (right column) for final snowfall patterns with a straight deflection fins (yellow) increasing in height from 1.34m (a) through 5.34m (d) placed 1.1 m away from the building.

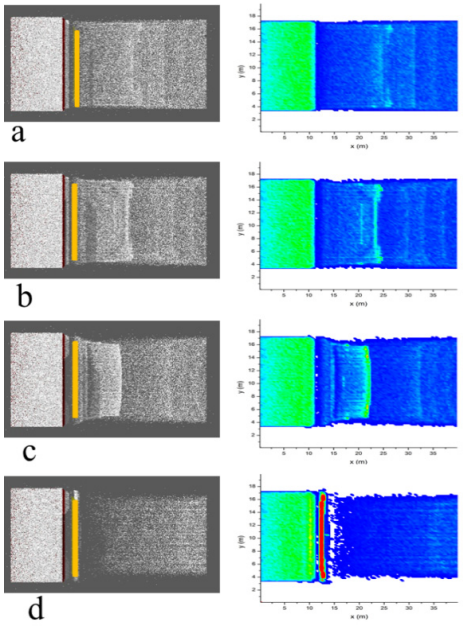

Figure 5. Visual renderings (left column) and contour maps (right column) for final snowfall patterns with a straight deflection fins (yellow) increasing in height from 1.34m (a) through 5.34m (d) placed 2.2 m away from the building.

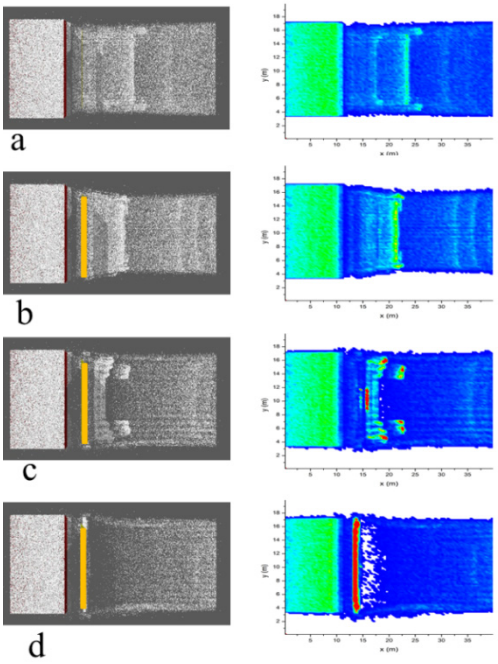

Fig. 6. Visual renderings (left column) and contour maps (right column) for final snowfall patterns with a straight deflection fins (yellow) increasing in height from 1.34m (a) through 5.34m (d) placed 3.3 m away from the building.

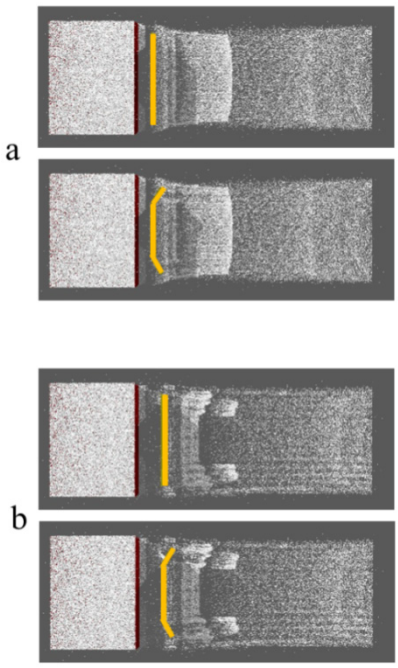

Fig. 7. Visual renderings comparing final snowfall patterns for straight and bent deflection fins (yellow) of height 4m placed (a) 2.2 m and (b) 3.3 m away from the building.

Because of the three dimensional nature of the simulations, the effects of bent fins were examined. In this study, straight fins occupy a constant x value but for bent fins the edges angle towards the center of the

system. Regardless of the effectiveness of the straight fin whose center is the same distance from the building as the bent fin, the bending has virtually no effect on snowdrift relocation. However, Fig. 7 shows that the bent edges have a secondary effect, crating shadows in the relocated drifts. So, the simulations presented here suggest that bent fins could be used to smooth or selectively shape relocated drifts from the deflection fin.

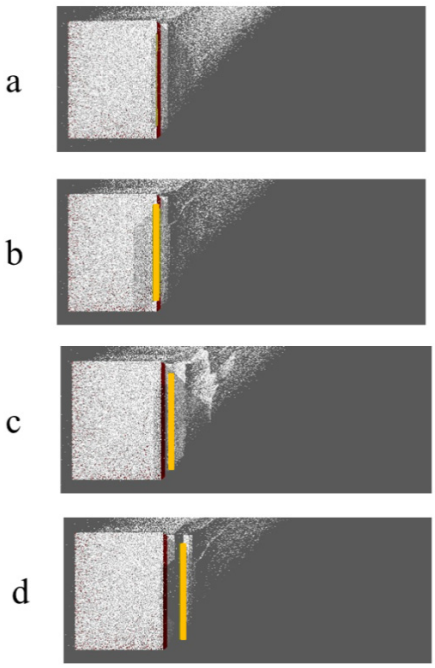

Fig. 8. Visual renderings for final snowfall patterns without a deflection fin (a) and with selected fins (yellow) having typical effects of shadowing and structure in the drifting (a-c).

In addition to bent fins the simulations were able to incorporate side winds, by creating a pressure gradient in the y – direction; Fig. 8 illustrates some typical final snowfall profiles for such simulations. For side gusting, lateral pressure differentials were scaled relative to those in the x – direction so that pressure gradients gave maximum wind speeds comparable to those in the x – direction, hence the 45 degree angle made by the snow edge off the horizontal in Fig. 8. The building itself created a shadow in the drift pattern and the fin creates an enhanced shadow as well as some structure in the pattern. Depending on where the fin is placed as well as its size, very intricate and complicated drifting patterns can be created.

4. CONCLUSION

Several conclusions from this work can be reached.

(*i*) Fins of intermediate size (3m – 4m in height) placed about 2 m – 3 m from the building have the best potential for problematic drift relocation.

(*ii*) Bent fins don't affect drift relocation significantly but does create shadows in relocated drifts and could be used to manipulate them.

(*iii*) Side winds result in drift shadowing patterns and interesting drift structures which can be controlled by manipulating the deflection fin the results could prove very useful in situations where the building architecture is asymmetric. Certainly more investigation of the effects of crosswinds is warranted.

ACKNOWLEDGEMENTS

We gratefully acknowledge fruitful discussions with and support from the UNI Facilities and Maintainance group.

REFERENCES

Akiyoshi, Serine, Masayuki, Shimura, Akira, Maruoka, Hirokazu, Hirano (1999). The Numerical Simulation of Snowdrift around a Building. *Int. J. Comp. Fluid Dynamics* 12(3), 249 – 255.

Beyers, Meiring and Waechters, Bill (2008). Modeling transient snowdrift development around complex three-dimensional structures. *J. Wind Eng. Ind. Aerodyn*. 96, 1603–1615.

Beyers, P.A. and T.M. Sundsbų (2004). Numerical simulation of three-dimensional, transient snow drifting around a cube. *Journal of Wind Engineering* 92(9), 725-747.

De Chant, Lawrence (2005). The venerable 1/7th power law turbulent velocity profile: a classical nonlinear boundary value problem solution and its relationship to stochastic processes. *Appl. Math. Comput.* 161, 463–474.

Doorschot, J., N. Raderschall and M. Lehning (2001, January). Measurements and one-dimensional model calculations of snow transport over a mountain ridge. *Annals of Glaciology* 32(1), 153-158.

Kim, D.H. and H.E. Rohde (1992, March). Modelling of Snowdrift Around Prismatic Buildings for Antarctic Environment. *J. Offshore and Polar Engineering* 2(I).

Lehning, M., J. Doorschot and C. Fierz and references therein (2002). A 3D model for snow drift and snow cover development in steep alpine terrain. *International Snow Science Workshop Penticton*, B.C (eds) .

Lehning, M., J. Doorschot, Raderschall and N Combining (2000). *Combining snow drift and SNOWPACK models to estimate snow loading in avalanche slopes.* Snow Engineering, Hjorth-Hansen, Holand, Leset & Norem (eds), 113-121.

Maldonado, E. and M.W. Roth (2012, submitted). Direct two–phase numerical simulation of snowdrifts external to building walls and remediation with deflection fins. *J. Wind Eng. Ind. Aerodyn.*.

Matyk, Maciej (2012). Solution to two-dimensional Incompressible Navier-Stokes Equations with SIMPLE, SIMPLER and Vorticity-Stream Function Approaches, Driven-Lid Cavity Problem: Solution and Visualization. http://citeseerx.ist.psu.edu/viewdoc/download?doi=10.1.1.14.5634&rep=rep1&type=url&i=0

Schneiderbauer, S., T. Tschachler, J. Fischbacher, W. Hinterberger and P. Fischer (2008). Computational fluid dynamic (CFD) simulation of snowdrift in alpine environments, including a local weather model, for operational avalanche warning. *Annals of Glaciology* 48(1), 150-158.

Sundsbø , P.A. (1998). Numerical simulations of wind deflection fins to control snow accumulation in building steps. *J. Wind Eng. Ind. Aerodyn*. 74-76, 543-552.

Sato, T., K. Kosugi, S. Mochizuki and M. Nemoto (2008). Wind speed dependences of fracture and accumulation of snowflakes on snow surface. *Cold Regions Science and Technology* 51, 229–239.